

EFFECT OF THE FIELD MAPS ON THE BEAM DYNAMICS OF THE ESS DRIFT TUBE LINAC

R. De Prisco*, ESS, Lund, Sweden and Lund University, Lund, Sweden
 M. Eshraqi, Y. I. Levinsen, R. Miyamoto, E. Sargsyan, ESS, Lund, Sweden
 A. Karlsson, Lund University, Lund, Sweden

Abstract

In the beam dynamics design and modelling of the European Spallation Source (ESS) Drift Tube Linac (DTL) simplified models have been used for the focusing and accelerating elements. Since the high current requires precise control of the beam to analyze the losses it is useful to perform the beam dynamics simulations by using accurate field maps of the focusing and accelerating elements. In this paper the effects of the 3D-field maps on the beam dynamics of the ESS DTL are presented.

INTRODUCTION

The ESS DTL is an in-kind contribution from INFN/LNL [1]. Five Radio Frequency (RF) cavities (tanks) are used to accelerate a proton beam of 62.5 mA from 3.62 MeV to 89.68 MeV at 352.21 MHz; the transverse focusing system is composed by Permanent Magnet Quadrupoles (PMQs) arranged in a F0D0 lattice.

RF FIELD MAP OF THE ESS DTL

The design of the ESS DTL is defined in [2]. The cell numbers (and, consequently, the tank lengths) and the average electric accelerating field, E_0 , are optimized simultaneously such that the sum of the power transferred to the beam, P_B , and the dissipated power on the internal tank surface, P_{Cu} , (including, on the last one, a factor 1.25 over the MDTfish computation) are slightly below 2.2 MW, that is the available RF power, P_{TOT} , per tank. The DTL parameters are summarized in Table 1 (E_{out} is the output energy of the beam at the end of each tank).

Table 1: DTL Parameters in Each Tank

Tank	1	2	3	4	5
E_0 [MV/m]	3.00	3.16	3.07	3.04	3.13
Cells	61	34	29	26	23
L_T [mm]	7618	7101	7583	7847	7687
P_B [kW]	1104	1114	1106	1064	1005
P_{Cu} [kW]	1088	1078	1090	1126	1190
P_{TOT} [kW]	2192	2191	2196	2189	2195
E_{out} [MeV]	21.29	39.11	56.81	73.83	89.68

Ideal and Nominal Accelerating Field

We define the average electric accelerating field, E_0 , reported in the Table 1, as the *ideal* accelerating field, from

* renato.deprisco@esss.se

now $E_{0,id}$. Even if all the cells, different in length, have the same frequency, *the accelerating field integral, cell by cell, is not constant* because of the imperfect mode matching between the adjacent cells. Thanks to algorithm presented in [3] it is possible to modify the geometry of the Drift Tubes (DTs) in order to calculate the electromagnetic field, solution of the Maxwell equations, inside each tank, such that the accelerating field is close to the ideal one. We call this field the *nominal* accelerating field, $E_{0,nom}$, shown in Fig. 1. From this moment all results are referred to the nominal accelerating field.

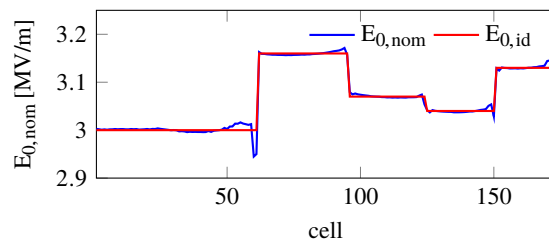


Figure 1: Nominal accelerating field in the DTL.

Self Perturbation Phenomena of the Post Couplers

The frequency perturbation due to the drift tube stems and the power couplers is compensated by tuning the cell face angles. Doing that the nominal accelerating field is achieved in the ESS DTL. Post Couplers (PCs) are used to stabilize the on axis accelerating electric field against tilts produced by mechanical errors (that, locally and randomly, change the resonant frequency of each cell). We define the *optimum lengths* of the PCs as the lengths for which there is the *confluence* [3]. The local frequency shift, due to the inserted PCs with their optimum lengths, must be compensated to avoid the *self perturbation* phenomena: uncompensated PCs produce, themselves, additional tilts of the accelerating electric field against which they are inserted.

FIELD MAP OF THE PMQs

The PMQ design is a modification of the segmented Halbach quadrupole.

The magnetic field into the beam pipe is given by the superposition of the magnetic fields of 16 parallelepiped permanent magnets of Sm_2Co_{17} . A transverse section of the PMQ is shown in Fig. 2. In each PMQ all the magnets (grey rectangles) have the same remanent magnetization along the appropriate direction.

The external radius of the PMQ housing is 30 mm. The transverse area of each of the 16 magnets is $w_m \times b_m =$

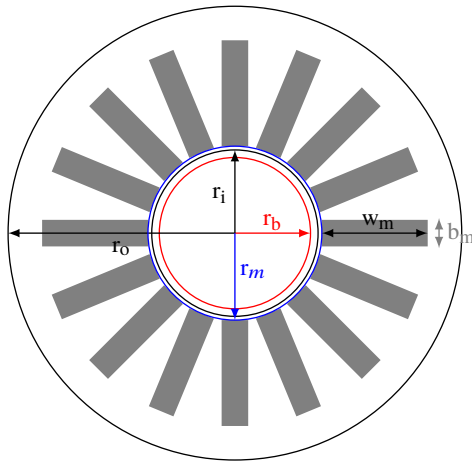


Figure 2: Transverse section of the PMQ.

14 mm × 4 mm. The other main transverse parameters are shown in Fig. 2 and the longitudinal PMQ lengths, L , are listed in Table 2 for the 5 tanks.

Table 2: PMQ Geometric Parameters

	r_b [mm]	r_i [mm]	r_m [mm]	L [mm]
Tank 1	10	11	11.5	50
Tank 2 and 3	11	12	12.5	80
Tank 4 and 5	12	13	13.5	80

Fringe Field of the PMQs

The hard-edge model, used in [2], assumes that the magnetic field changes steplike at the border of the magnet (B_H in Fig. 3), while in reality it changes smoothly and fringes outside the magnet (B_F in Fig. 3).

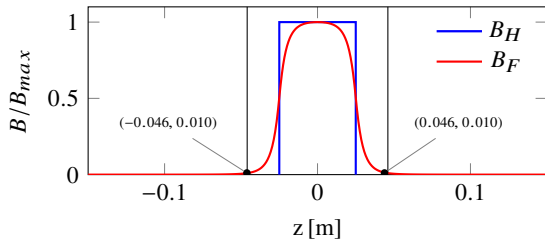


Figure 3: Magnetic field for the PMQ of 50 mm at r_b .

The longitudinal effective length, L_{eff} , defined in (1) is equal to 50.6 mm and to 80.2 mm for the PMQ of length 50 mm and 80 mm respectively.

$$L_{\text{eff}} = \frac{1}{B_{F,\text{max}}(r_b)} \int_{-\infty}^{\infty} B_F(r_b, z) dz. \quad (1)$$

BEAM DYNAMICS WITH FIELD MAPS

Once the field maps of all focusing and accelerating element are defined, it is possible to transport the beam through

the DTL. The input beam distribution is generated as described in [4]. The input section is 75 mm before the first PMQ in order to take in account its fringe field. A preliminary tuning on the input phase of the RF field map of each tank is done in order to reach the design beam energy at the end of each tank, E_{out} (Table 1). Then a fine tuning on the input phases of the RF field maps is performed in order to smooth the longitudinal dynamics. From now all the calculation are done when the focusing and the accelerating elements are described both by their field maps and by their matrices; the results are subscripted with F and M respectively. In the matrices, that describe the PMQs, the calculated effective lengths are taken into account.

Evolution of the beam phase spread is shown in Fig. 4.

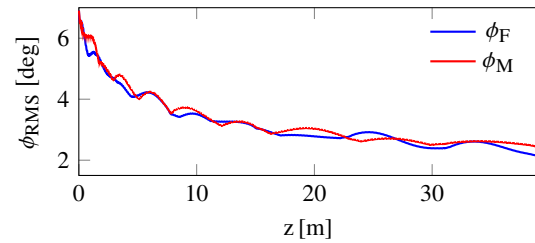


Figure 4: RMS Beam Phase Spread at 352.21 MHz.

The main beam parameters at the end of each tank are reported in Table 3.

Table 3: Twiss Parameters (black colour is referring to the field map, red colour to the matrices) at the End of Each Tank (β is expressed in mm/ π .mrad, ϵ is expressed in π .mm.mrad)

Twiss \ Tank	1	2	3	4	5
α_x	-2.81	-2.11	2.42	-2.22	-2.27
	-2.72	-2.05	2.53	-2.29	-2.42
β_x	1.78	2.23	4.03	4.36	5.22
	1.76	2.18	4.24	4.42	5.38
ϵ_x	0.298	0.293	0.293	0.296	0.296
	0.298	0.294	0.293	0.293	0.294
α_y	2.11	3.29	-1.76	2.31	2.48
	2.11	3.47	-1.92	2.23	2.40
β_y	1.49	3.58	2.84	4.59	4.90
	1.50	3.10	3.02	4.58	4.85
ϵ_y	0.287	0.293	0.298	0.302	0.298
	0.288	0.291	0.297	0.296	0.298
α_z	-0.28	0.04	-0.13	-0.16	0.10
	-0.21	0.06	0.02	0.14	0.19
β_z	1.71	2.99	4.75	5.43	5.76
	1.81	3.10	4.34	5.79	6.51
ϵ_z	0.384	0.385	0.385	0.379	0.392
	0.381	0.385	0.385	0.383	0.383

From this moment, for brevity, we will refer only to the first tank, but similar studies are done for all the tanks.

Content from this work may be used under the terms of the CC BY 3.0 licence (© 2015). Any distribution of this work must maintain attribution to the author(s), title of the work, publisher, and DOI.

Natural Emittance Growth

The transverse *natural* [4] emittances are overlapping along the first tank for both field map and matrix representation. The longitudinal *natural* emittances, instead, are overlapping in the first 2 m, then their difference increases up to 1 % at the end of the tank 1 as shown in the Fig. 5.

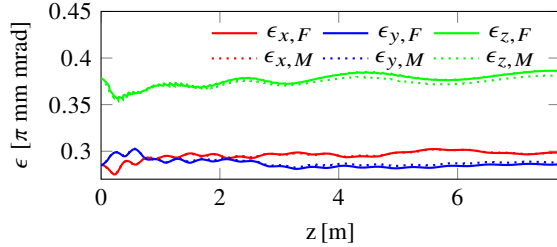


Figure 5: Emittance in x (red), y (blue) and z (green).

Klystron Sensitivity

Figure 6 shows the additional emittances when the klystron phase, ϕ_k , is changed from its nominal value.

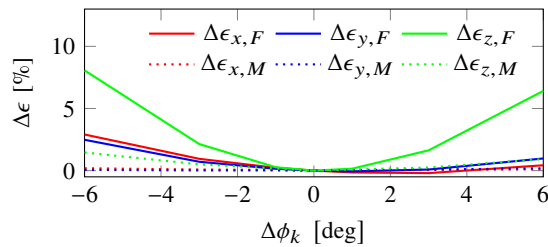


Figure 6: Additional Emittance Growth in x (red), y (blue) and z (green) as a function of klystron phase.

Figure 7 shows the additional emittances when the klystron amplitude, E_k , is changed from its nominal value.

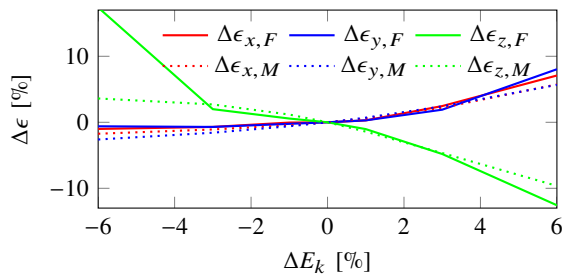


Figure 7: Additional Emittance Growth in x (red), y (blue) and z (green) as a function of klystron amplitude.

Error on the Cell Accelerating Field

The manufacturing errors induce a random shift of the resonant frequency in each cell. As explained in [3], a frequency perturbation in one cell induces a tilt that affects the accelerating field in *all* cells of the same tank. Assuming a random frequency error in each cell (due to the mechanical

tolerances of the cell components) of one tank the electromagnetic field can be calculated by solving the Maxwell equation inside the tank. 500 field maps per each tank are generated by using MDTfish with a maximum error on the accelerating field, in modulus, equal to 1%. The average additional emittance growth is 1%, 2% and 2% respectively in the XX', YY' and ZZ' plane. When the accelerating elements are described by their matrices, instead, this type of error is analysed by introducing a random and independent error on the amplitude of each cell (uniformly distributed between -1% and 1% over 500 cases). The average additional emittance growth is negligible in the XX', YY' and less than 0.5% in the ZZ' plane.

CONCLUSION

The nominal beam dynamics of the ESS DTL is analyzed when the focusing and the accelerating elements are described both by their field maps and by their matrices. The differences of transverse natural emittances, at the end of tank 5, are 0.7 % in the XX' plane and 2.3 % in the ZZ' plane. No difference is detected in the YY' plane.

The klystron phase sensitivity study shows a difference of the additional emittance growths that is, in modulus, less than 0.2% in all the planes, if the klystron phase changes by less than ± 1 deg. The difference becomes huge outside of this range.

The klystron amplitude sensitivity study shows a difference of the additional emittance growths that is, in modulus, less than 0.4 %, 0.9 % and 0.7 %, respectively in XX', YY' and ZZ' plane, if the klystron amplitude changes by less than ± 3 %. The difference becomes huge outside of this range.

The error of the cell accelerating field induces an additional average emittance growths of 1 %, 2 % and 2 %, respectively in XX', YY' and ZZ' plane, in the case of field map. When the focusing and the accelerating elements are described by matrices, instead, the transverse additional emittance growths, due to the cell to cell error, are negligible; the longitudinal one is 0.5 %. This difference is essentially due to the different methods to model this error: random and independent cell amplitude errors don't respect the Maxwell equation.

REFERENCES

- [1] F. Grespan *et al.*, "ESS DTL Design and Drift Tube Prototypes," in *Proc. LINAC'14*, Geneva, Switzerland, Sep. 2014, paper THPP087, p. 1050.
- [2] R. De Prisco *et al.*, "ESS DTL Status: Redesign and Optimizations," in *Proc. IPAC'14*, Dresden, Germany, Jun. 2014, paper THPME041, p. 3314.
- [3] R. De Prisco *et al.*, "ESS DTL RF Modelization: Field Tuning and Stabilization," in *Proc. IPAC'13*, Shanghai, China, May 2013, paper THPWO070, p. 3918.
- [4] R. De Prisco *et al.*, "Error Study on Normal Conducting ESS LINAC," in *Proc. LINAC'14*, Geneva, Switzerland, Sep. 2014, paper THPPO042, p. 942.